

Investigating acoustic-induced deformations in a foam using multiple light scattering

M. Erpelding, R. M. Guillermic, B. Dollet, A. Saint-Jalmes, and J. Crassous*

Institut de Physique de Rennes, UMR CNRS 6251, Université de Rennes 1, Campus de Beaulieu, F-35042 Rennes Cedex, France

(Received 19 January 2010; revised manuscript received 8 June 2010; published 27 August 2010)

We have studied the effect of an external acoustic wave on bubble displacements inside an aqueous foam. The signature of the acoustic-induced bubble displacements is found using a multiple light scattering technique, and occurs as a modulation on the photon correlation curve. Measurements for various sound frequencies and amplitudes are compared to analytical predictions and numerical simulations. These comparisons finally allow us to elucidate the nontrivial acoustic displacement profile inside the foam; in particular, we find that the acoustic wave creates a localized shear in the vicinity of the solid walls holding the foam, as a consequence of inertial contributions. This study of how bubbles “dance” inside a foam as a response to sound turns out to provide new insights on foam acoustics and sound transmission into a foam, foam deformation at high frequencies, and analysis of light scattering data in samples undergoing nonhomogeneous deformations.

DOI: [10.1103/PhysRevE.82.021409](https://doi.org/10.1103/PhysRevE.82.021409)

PACS number(s): 83.80.Iz, 42.25.Dd, 78.35.+c, 62.20.F–

I. INTRODUCTION

Inside an aqueous foam, bubbles are highly packed and compressed on each other. They are jammed, and cannot move apart by themselves. Nevertheless, bubbles are soft objects, and can easily be distorted: consequently, their shape, position and topology (numbers of neighbors) are never irreversibly frozen. Foam coarsening is a first mechanism which modifies the organization of bubbles inside the foam [1,2]. This coarsening results from gas diffusion from bubbles to others; some bubbles grow and others shrink, which induces a constant modification of the bubbles shapes. To conserve the local mechanical equilibrium, some discrete bubble rearrangements must be induced as a consequence of coarsening. The evolution with time of the rate of bubble rearrangements and of the mean bubble radius have been studied by many techniques, in particular multiple light scattering ones such as diffusing-wave spectroscopy (DWS) [3]. On long time scales (low frequencies), the aging of the foam due to coarsening is finally able to unjam the bubbles, fully relaxing any applied stress so that a foam behaves as a viscous fluid [4].

Applying a shear stress is another way to modify the bubbles shapes and organization. Small shear oscillations are classically used to determine the viscoelastic moduli in the linear regimes [5]. Under small shear stresses, the bubbles only slightly distort and are able to store some energy. As a consequence, a foam creeps like an elastic solid with a shear storage modulus G' typically ten times larger than the viscous one G'' . The quantitative values depend on both the physical and chemical foam properties [6–8]. Increasing the shear stress—above a yield value—can also lead to irreversible bubble rearrangements, and to the continuous flow of the foam. As for coarsening, bubbles can be unjammed by shear, and techniques like DWS have also been useful to capture the links between macroscopic properties and bubble-scale effects [6,9,10].

Despite the large research activity in this field, foam rheology remains a complex topic, with many open issues. The

full dependence with amplitude and frequency of the viscoelastic moduli is complex and not fully understood, especially at low and high frequencies [4,11]. Under continuous shear, questions on localization, definition of yield stress or wall slip are also still pending. As well, one has to figure out the coupling between effects occurring at different length scales, and the impact of the interfacial physical chemistry on the macroscopic features. An important motivation of studying foam rheology also comes from the fact that many features observed for foams (jamming and yielding, slow relaxation and aging) are often recovered in many other soft glassy materials such as emulsions, pastes, or concentrated colloidal suspensions. In that respect, an aqueous foam can be considered as a possible model system illustrating the whole class of jammed systems. As a consequence, another active axis of research deals with the construction of general constitutive laws valid for all these soft systems [12–15].

In order to bring new clues, finding some other ways of externally soliciting a foam is a possible approach. Unaccessible ranges of deformations or frequencies, as well as new regimes, could then be investigated. Here, we explore the effect of an external acoustic wave on the bubbles inside a foam, and whether it can be used as an interesting mode of solicitation for investigating bubble deformation and foam mechanics at high frequencies. Though an acoustic perturbation has already been used to study the rheology of colloids with ultrasonic frequencies [16], it has never been used for studying the rheology of dispersed systems like aqueous foams. In fact, it is similar to shear as amplitude and frequencies can be varied, but here much higher frequencies than in classical rheometers can be obtained [17]. Another motivation for studying the effect of a sound wave on a foam is the foam acoustics itself: although foams exhibit rather unusual acoustic properties, not much has been done on the topic of sound propagation inside them. As a matter of fact, experimental results on acoustics of foams mostly deal with speed of sound and wave attenuation [18], while almost no results are reported on the local motion of the bubbles and on the coupling between foam elasticity and sound wave propagation. In this paper, we show that coupling an acoustic signal (as a “source”) and a multiple light scattering signal (as a “detector”) turns out to shed lights on wall slip, on shear

*jerome.crassous@univ-rennes1.fr

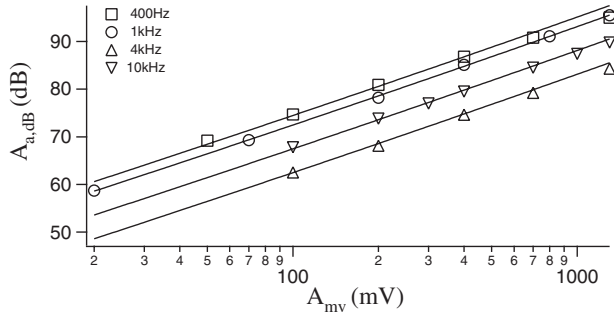


FIG. 1. Measured acoustic amplitude (dB) as a function of the amplitude (mV) of the input signal in the loudspeaker. Different symbols correspond to different frequencies. Solid lines are guide-lines with slopes of 20 dB/decade.

viscoelasticity, on acoustics, and on shear profiles and how to measure them in a range of frequencies and deformations usually not accessible.

II. EXPERIMENTAL SECTION

Our samples are made of commercial shaving foam (Gillette) poured into a U-shaped polyvinyl chloride (PVC) cell with transparent glass walls. The inner dimensions of the cell are $(36 \times 41 \times 17)$ mm³ in the x , y , and z directions, respectively (see Fig. 2).

To produce an acoustic perturbation, a loudspeaker (Jeu-lin) is fixed approximately 45 cm above the foam. It receives a sinusoidal input signal of controlled amplitude A_{mV} and frequency f from a function generator. We have used frequencies of 400 Hz, 1 kHz, 4 kHz, and 10 kHz. For each of these values, we have measured the acoustic amplitude $A_{a,dB}$ of the sound waves in air as a function of A_{mV} using a sonometer (Lutron SL-4001). As expected, $A_{a,dB}$ varies linearly with A_{mV} with a slope of 20 dB/decade (Fig. 1).

The resulting acoustic displacements A_a in air can be computed from the data as:

$$A_a = \frac{P_0}{\rho_a c_a \omega} 10^{A_{a,dB}/20}, \quad (1)$$

where $A_{a,dB}$ is the measured acoustic amplitude in air in decibels, ρ_a is the density of air and c_a is the celerity of sound in air at ambient temperature and atmospheric pressure, $\omega = 2\pi f$ is the pulsation of the acoustic wave, and $p_0 = 20 \mu\text{Pa}$ the reference pressure from the definition of a decibel.

As mentioned in the introduction, light scattering has been used to study coarsening-induced or shear-induced effects. Here, we have used DWS to examine the deformation of a foam by an acoustic wave. Light scattering techniques are classical tools to investigate the structure and dynamics of random media. They consist of illuminating a diffusing sample with coherent light, and analyzing the intensity fluctuations of the transmitted or backscattered light. These fluctuations arise from the modification of the optical paths followed by photons propagating inside the sample, due to its internal dynamics or to an externally imposed deformation.

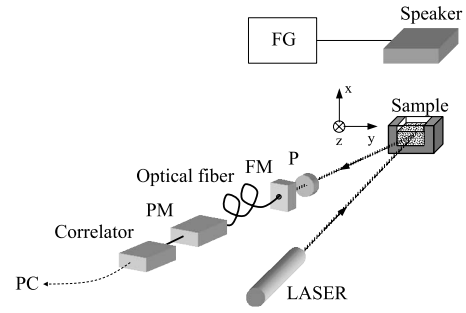


FIG. 2. Sketch of the experimental setup. The laser beam illuminates the center of the foam sample. A monomode optical fiber fixed on a fiber mount (FM) carries the backscattered light into a photomultiplier tube (PM). The polarizer (p) ensures us that only one direction of the depolarized backscattered light is collected. The signal is then analyzed by a linear correlator. Acoustic waves are generated by the loudspeaker fixed above the foam that receives a sinusoidal input signal from a function generator (FG).

In the multiple scattering limit, light propagation in random media can be described as a random walk in the diffusion approximation. Then, the intensity fluctuations of the output light can be related to deformations of the sample [19–21].

Here, the sample is illuminated with an unpolarized HeNe laser beam of wavelength $\lambda = 633$ nm, beam diameter 0.8 mm and power 5 mW. The backscattered light is collected after a linear polarizer and propagates through a monomode optical fiber into a photomultiplier tube. The output signal is then analyzed by a linear correlator (correlator.com Flex02–12D/C). Figure 2 shows a sketch of the experimental setup.

Experiments are organized as follows: after pouring the foam into the cell, we systematically wait for approximately one hour before starting the measurements [3]. Then, for a given frequency and amplitude of the acoustic signal, we record the correlation function $g_2(\tau)$ of the backscattered light intensity I between times t and $t + \tau$.

$$g_2(\tau) = \frac{\langle I(t)I(t + \tau) \rangle}{\langle I(t) \rangle \langle I(t + \tau) \rangle}, \quad (2)$$

where $\langle \cdot \rangle$ represents a temporal average over the duration of the measurement. In our case, measurements always last 2 min. Successive measurements on a given sample are all performed within half an hour. This ensures us that the foam does not age significantly during the experiment.

In the absence of acoustic perturbation, $g_2(\tau)$ decreases monotonically with τ due to the coarsening of the foam, as shown on the inset of Fig. 3. When we add the acoustic perturbation, we observe a modulation of $g_2(\tau)$, i.e., a succession of partial decorrelations and recurrences that adds up to the decorrelation observed in the absence of acoustic perturbation. This shows that in addition to aging, the foam is cyclicly deformed by the acoustic wave (see Fig. 3).

We observe that for all frequencies, the amplitude of the modulation increases with the amplitude of the acoustic wave. As an example, we plot on Fig. 3 the typical measured $g_2(\tau)$ at a fixed frequency $f = 400$ Hz for two different acoustic amplitudes $A_{a,dB} = 90.8$ and 80.9 dB.

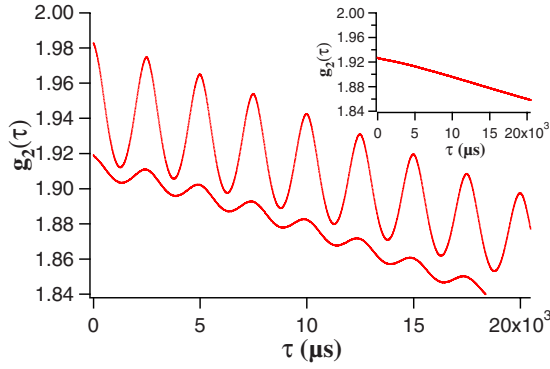


FIG. 3. (Color online) Examples of measured $g_2(\tau)$ when the foam is submitted to acoustic waves of frequency 400 Hz and amplitudes 90.8 dB (upper curve) and 80.9 dB (lower curve). Inset: Typical $g_2(\tau)$ measured in the absence of acoustic perturbation.

Moreover, in the range $\tau < 20 \times 10^{-3}$ s, the amplitude of the modulation is roughly constant with τ , signing reversibility of the displacement. Indeed, although irreversible bubble rearrangements could be induced by the acoustic wave, yielding a decrease of the modulation of $g_2(\tau)$ with time, we are in an experimental situation in which the foam has been submitted to a large number of acoustic oscillations before we perform the measurement. As a consequence, these effects, arising shortly after the acoustic perturbation is turned on, are not relevant here. Furthermore, the acoustic displacements are always small compared to bubbles sizes (see Sec. IV B), so that plastic effects are expected to be negligible.

We now examine the effect of the cell walls on the response of the foam to the acoustic perturbation. To eliminate the effect of the lateral walls, the foam is now poured directly onto a horizontal PVC plate, instead of into the U-shaped cell. Furthermore, one has to be aware that in DWS experiments on foams, the volume over which the deformation is probed increases with the age of the foam. Indeed, since the bubbles size increases when the foam ages, it becomes more and more transparent so that light propagates inside over an average distance that increases with the age of the foam before being backscattered [3]. For this reason, these experiments dealing with the effects of the walls have to be performed shortly after preparing the foam, which is then opaque enough in order not to probe the deformation in the vicinity of the bottom boundary. We fix the frequency and amplitude of the acoustic signal. First, we observe a significant decrease of $g_2(\tau)$ with τ , due to the fact that the foam sample is “young” so that it ages faster than in the situation of Fig. 3. Second, almost no modulation is observed on $g_2(\tau)$ (bottom curve on Fig. 4). Then, for the same acoustic perturbation, we add a glass wall against the illuminated side of the foam sample and observe a clear modulation of $g_2(\tau)$ (top curve of Fig. 4). As explained later, this may be understood by the fact that the stress generated by the acoustic wave at a foam/air interface is likely lower than the one generated at a foam/glass wall interface.

III. LIGHT SCATTERING MODEL

Our experiments show that the foam is deformed when submitted to an acoustic perturbation. In this section, we

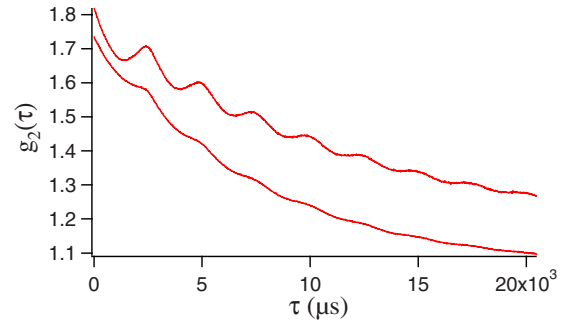


FIG. 4. (Color online) Correlation functions $g_2(\tau)$ measured for the same acoustic perturbation in the presence (top curve) and in the absence (bottom curve) of wall on the illuminated side of the foam sample. The frequency and amplitude of the acoustic wave in both cases are 400 Hz and 82.3 dB.

propose a theoretical framework describing the effect of an acoustic wave on the backscattered light correlation functions, for a foam constrained between solid walls. We impose that the foam displacement vanishes at the solid wall, which is justified later in Sec. IV B. First, we propose analytical expressions of the correlation function at small acoustic displacements. Then, we report the results of numerical simulations.

A. Variation of the electric field autocorrelation function g_1 with the acoustic amplitude

The effect of an acoustic perturbation on the coherence of light multiply scattered by a medium has been the subject of some theoretical and experimental studies. The basic mechanism has been identified in [16] by considering the light scattered by a colloidal suspension in which ultrasonic waves propagate. This propagation induces a deformation of the sample, modifying the optical paths inside. In [16], the propagation of a high-frequency (2 MHz) ultrasonic wave is considered. In this case, the deformation of the material arises from its small compression and dilation along the direction of propagation of the acoustic wave and then scales with the acoustic frequency.

In our experiment, we analyze backscattered light, thus we measure the acoustic deformation of the foam mostly near its boundary. In the following, we make the assumption that the deformation caused by the propagation of an acoustic wave has a vanishing amplitude at the solid wall (no-slip boundary condition), as will be justified in Sec. IV B.

We consider a simplified model for the propagation of a photon inside the foam: it consists of a random walk made of a succession of independent steps separated by a constant scattering mean free path l . We also consider that the directions of the different steps are uncorrelated. This makes the transport mean free path $l^* = l$. Figure 5 schematically represents this random walk. We note $\mathbf{A}_f(\mathbf{r}, t)$ the acoustic displacement of the foam, where \mathbf{r} is the position in the foam and t is the time.

We assume that the distance between scattering events (see Fig. 5) is large compared to the optical wavelength λ and that there is no correlation between different paths (weak

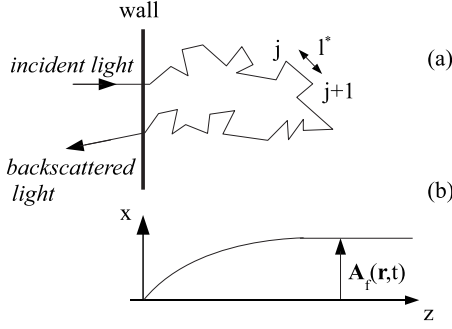


FIG. 5. (a) Schematic drawing of the random walk propagation of light in the foam in a backscattering geometry. (b) Representation of the acoustic displacement $\mathbf{A}_f(\mathbf{r}, t)$.

scattering approximation). Then the autocorrelation function of the scattered electric field $\mathbf{E}(t)$ is [22–24]:

$$g_1(\tau) = \langle \mathbf{E}(t) \cdot \mathbf{E}^*(t + \tau) \rangle_t = \int_s P(s) \langle \mathbf{E}_s(t) \cdot \mathbf{E}_s^*(t + \tau) \rangle_{t,s} ds, \quad (3)$$

where we have decomposed the electric field into different components \mathbf{E}_s from the light scattered along paths of length s . $P(s)$ is the path length distribution, $\langle \cdot \rangle_t$ represents a temporal average, and $\langle \cdot \rangle_{t,s}$ represents an average over both time and paths of length s . For clarity, in the following we will only consider the acoustic-induced motion of the foam. As already mentioned, foam bubble rearrangements arising spontaneously during aging, or induced by the acoustic perturbation, will contribute to the decorrelation of the scattered field. Again, this decorrelation, shown on the inset of Fig. 3 simply adds to the modulation induced by the acoustic wave.

The autocorrelation function along a path of length s is [16,22,23]:

$$\langle \mathbf{E}_s(t) \cdot \mathbf{E}_s^*(t + \tau) \rangle_{t,s} = \left\langle \exp \left[-i \sum_{j=1}^{j=s/l^*} \Delta \phi_j(t, t + \tau) \right] \right\rangle, \quad (4)$$

where $\Delta \phi_j(t, t + \tau)$ is the phase variation for the light wave propagating between two successive scattering events at \mathbf{r}_j and \mathbf{r}_{j+1} and between times t and $t + \tau$. If we note \mathbf{e}_j the unit vector joining the points \mathbf{r}_j and $\mathbf{r}_{j+1} = \mathbf{r}_j + l^* \mathbf{e}_j$, we have:

$$\Delta \phi_j(t, t + \tau) \simeq k \mathbf{e}_j \cdot [\mathbf{A}_f(\mathbf{r}_{j+1}, t + \tau) - \mathbf{A}_f(\mathbf{r}_j, t + \tau)] - k \mathbf{e}_j \cdot [\mathbf{A}_f(\mathbf{r}_{j+1}, t) - \mathbf{A}_f(\mathbf{r}_j, t)], \quad (5)$$

where $k = 2\pi/\lambda$ is the light wave vector. Given the geometry of the experiment, we consider an acoustic displacement given by:

$$\mathbf{A}_f(\mathbf{r}_j, t) = A_f(z) \sin(\omega t) \mathbf{e}_x. \quad (6)$$

In this expression, we have dropped the x dependency of the displacement amplitude $A_f(z)$. Indeed, we assume that the displacement varies over a distance of a few bubble diameters in the z direction (see Sec. IV B), while it only varies over an acoustic wavelength λ_{acc} in the direction x of propagation of the acoustic wave. In our case, the bubble size is of

order $D \approx 10^{-4}$ m, and taking the sound velocity in the foam $c \approx 50$ m/s [18], we have $\lambda_{acc} = c/f = 5$ mm for the highest frequency 10 kHz, and $\lambda_{acc} \geq 1$ cm for the other frequencies. It follows that the displacement differences involved in Eq. (5) along the x direction are negligible compared to variations along the z direction. The beam diameter and the scattering mean free path are small compared to λ_{acc} . So we can neglect an average of the deformation along the x direction.

Assuming that the displacement field varies slowly between two scattering events [i.e., $l^* dA_f(z)/dz \ll A_f(z)$], Eq. (5) becomes:

$$\Delta \phi_j(t, t + \tau) \simeq k l^* \mathbf{e}_{j,x} \mathbf{e}_{j,z} \frac{dA_f(z)}{dz} \times \{ \sin[\omega(t + \tau)] - \sin(\omega t) \}. \quad (7)$$

Averaging Eq. (7) over both time and scattering orientations, we obtain $\langle \Delta \phi_j(\tau) \rangle = 0$. Moreover, for an isotropic distribution of \mathbf{e}_j we have $\langle e_{j,x}^2 e_{j,z}^2 \rangle = 1/15$, and:

$$\langle \Delta \phi_j^2(\tau) \rangle = \frac{1}{15} k^2 l^{*2} \left(\frac{dA_f(z)}{dz} \right)^2 (1 - \cos(\omega \tau)). \quad (8)$$

For small deformations, we can expand Eq. (4):

$$\langle \mathbf{E}_s(t) \cdot \mathbf{E}_s^*(t + \tau) \rangle_{t,s} \simeq 1 - \frac{1}{2} \left\langle \left[\sum_{j=1}^{j=s/l^*} \Delta \phi_j(t, t + \tau) \right]^2 \right\rangle. \quad (9)$$

For an random walk with no correlation of scattering orientations, the phase variations $\Delta \phi_j(t, t + \tau)$ are independent variables, and then:

$$\begin{aligned} \langle \mathbf{E}_s(t) \cdot \mathbf{E}_s^*(t + \tau) \rangle_{t,s} &\simeq 1 - \frac{1}{2} \sum_{j=1}^{j=s/l^*} \langle \Delta \phi_j^2(\tau) \rangle \\ &\simeq \exp \left[- \sum_{j=1}^{j=s/l^*} \frac{\langle \Delta \phi_j^2(\tau) \rangle}{2} \right]. \end{aligned} \quad (10)$$

The quadratic average of the phase variations Eq. (8) depends on the local deformation $dA_f(z)/dz$. If the deformation is heterogeneous, i.e., if $dA_f(z)/dz$ depends on z , then $\langle \Delta \phi_j^2(\tau) \rangle$ implicitly depends of z . The problem of the z averaging of Eq. (8) for paths of length s in a heterogeneous deformation field has been studied in numerous papers [19,20,25,26]. The average of the deformation over the sample depends on both the geometry of lighting and light collection, and on the spatial repartition of the deformation.

The case of a homogeneous Couette flow has been addressed theoretically [19,20,26] and a homogeneous dilation has been considered in [27,28]. Poiseuille flow with heterogeneous deformation has been studied both experimentally [25,26] and theoretically [19,20,25,26]. More complex deformations fields have also been considered experimentally [21] and theoretically [19,20,26].

Within the assumptions made here, i.e., a deformation localized near a wall in a backscattering geometry, the situation is depicted on Fig. 6. Let ξ be the extent of the deformed zone in the z direction. If photons propagate in the foam

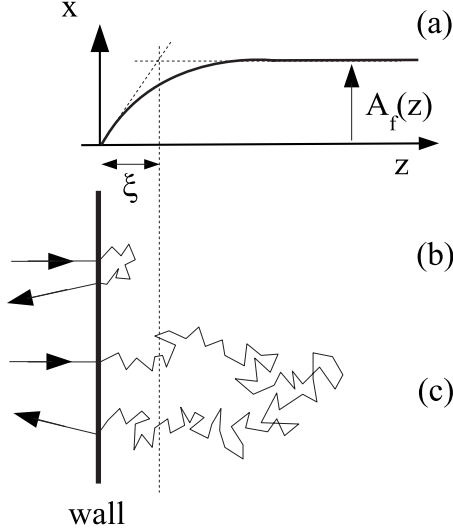


FIG. 6. (a) A deformation localized near a wall, extending over a characteristic distance ξ from the wall. (b) Short loops are subject to a constant deformation. (c) Long loops are deformed only near the wall.

following loops of small extent compared to ξ , then $\langle \Delta \phi_j^2(\tau) \rangle$ is independent of z [Fig. 6(b)]. On the opposite, if loops extend deeply inside the sample, only their small part for which $z \leq \xi$ is subject to deformation [Fig. 6(c)].

Following [19], we consider a displacement $A_f(z) = A_f \times [1 - \exp(-z/\xi)]$ along the x direction [see Fig. 6(a)]. We introduce $s^* = (3/4)(\xi^2/l^*)$, the length of the random walk needed to penetrate over a distance ξ inside the sample. If $s < s^*$, the path remains completely inside the sheared zone, and the deformation is $\approx A_f/\xi$ for each step of the random walk [Fig. 6(b)]. If $s > s^*$, only a part of length s^* of the path is deformed [Fig. 6(c)]. It follows that the variance $\langle \Delta \phi_s^2 \rangle = \sum_{j=1}^{s/l^*} \langle \Delta \phi_j^2(\tau) \rangle$ of the phase variation for paths of length s is [19]:

$$\begin{aligned} \langle \Delta \phi_s^2 \rangle &\approx \frac{1}{15} \left(\frac{k l^* A_f}{\xi} \right)^2 [1 - \cos(\omega \tau)] \frac{s}{l^*} \quad \text{if } s < s^* \\ &\approx \frac{1}{15} \left(\frac{k l^* A_f}{\xi} \right)^2 [1 - \cos(\omega \tau)] \frac{s^*}{l^*} \quad \text{if } s > s^*. \end{aligned} \quad (11)$$

Finally, computing the correlation function g_1 from Eq. (3) requires to know the path length distribution $P(s)$. This distribution is found by solving the diffusion equation for the density U of photons in the foam with the appropriate boundary conditions. We use standard mixed boundary conditions: $U - z_e(\partial U / \partial z) = 0$ at $z=0$, with z_e the extrapolation length [22–24]. For an air/glass/foam interface and with a foam liquid fraction $\varepsilon = 10\%$, it has been found experimentally that $z_e = 1.05 l^*$ [29]. We also consider that light begins to diffuse at a distance $z_0 \approx l^*$ inside the sample [30]. With these conditions, we find [30,31]:

$$P(s) \propto \sqrt{\frac{3}{\pi l^* s}} \exp\left(-\frac{3z_0^2}{4l^* s}\right) \left[1 - \frac{\exp(x^2) \operatorname{erfc}(x)}{z_e \sqrt{\frac{3}{\pi l^* s}}} \right], \quad (12)$$

with $x = \frac{z_0}{2} \sqrt{\frac{3}{s l^*}} + \frac{1}{z_e} \sqrt{\frac{s l^*}{3}}$.

The correlation function may then be calculated as:

$$g_1 = \int_{s=0}^{s=s^*} P(s) \exp\left(-\frac{s}{l^*} u\right) ds + \int_{s=s^*}^{s=\infty} P(s) \exp\left(-\frac{s^*}{l^*} u\right) ds, \quad (13)$$

with $u = \frac{1}{30} \left(\frac{k l^* A_f}{\xi} \right)^2 [1 - \cos(\omega \tau)]$.

In the limit $s^* u / l^* > 1$, Eq. (13) becomes $g_1 \approx \int_{s=0}^{s=\infty} P(s) \exp(-su/l^*) ds$, which is the Laplace transform of $P(s)$. This is $g_1 \approx \exp(-z_0 \sqrt{3u/l^*}) / (1 + z_e \sqrt{3u/l^*})$ [30,31]. If $z_0 \sqrt{3u/l^*} < 1$, $g_1 \approx 1 - (z_0 + z_e) \sqrt{3u/l^*}$. In the opposite limit $s^* u / l^* < 1$, g_1 differs from the Laplace transform of $P(s)$. The expansion of g_1 in the limit of small deformation is then obtained by numerical integration of Eq. (13). With $z_0 = l^*$ and $z_e = 1.05 l^*$, we find that $g_1 \approx 1 - 2.7 \sqrt{\frac{s^*}{l^*}} u$. To summarize, the expansions of g_1 are:

$$\begin{aligned} g_1(\tau) &\approx 1 - 0.078 k^2 A_f^2 \frac{l^*}{\xi} [1 - \cos(\omega \tau)] \\ &\quad \text{if } k A_f \sqrt{1 - \cos(\omega \tau)} < 1 \end{aligned} \quad (14)$$

$$\begin{aligned} &\approx 1 - 0.65 k A_f \frac{l^*}{\xi} \sqrt{1 - \cos(\omega \tau)} \\ &\quad \text{if } 1 < k A_f \sqrt{1 - \cos(\omega \tau)} < \frac{\xi}{l^*}. \end{aligned} \quad (15)$$

Equations (14) and (15) deserve some comments. Let us first discuss the limit $\xi \rightarrow \infty$: this corresponds to a constant shear $\Gamma = A_f / \xi$ in all the material. In this limit, the situation described by Eq. (14) does not occur, and $1 - g_1$ varies linearly with Γ in the limit $k l \Gamma \ll 1$, as predicted by Eq. (15). When the extent of the sheared zone ξ is finite, the situation is somewhat different. The decorrelation $1 - g_1$ at early delay times is dominated by the contribution of long photon paths in the medium [22,23]. However, these long paths being essentially in nondeformed parts of the material, the decorrelation is smaller than in the case of a homogeneous shear [32]. This is the situation described by Eq. (14). Nevertheless, when the deformation is large ($k A_f \gg 1$), all paths with lengths $s > s^*$ yield $\langle \Delta \phi_s^2 \rangle \gg 1$ [see Eq. (11)]. Then, $\exp(-\langle \Delta \phi_s^2 \rangle / 2)$ vanishes as if all paths—even long ones—were indeed sheared, so that $1 - g_1$ is the same as for a homogeneous shear.

B. Numerical simulations

The aim of this subsection is first to check Eqs. (14) and (15) with a numerical simulation of deformed random walks following the rules of Sec. III A. We will also consider random walks with correlated orientations of successive steps.

We first simulate photon propagation in the foam as a random walk of constant step length l^* , with no correlation of orientations. The random walk starts at $z=0$ with $\mathbf{e}_1 = \mathbf{e}_z$. After each step, \mathbf{e}_j is chosen with an isotropic orientation. The random walk finishes when $z < 0$. The path thus obtained is deformed according to Eq. (6), and the variation of the path length is calculated. For a fixed τ , the correlation

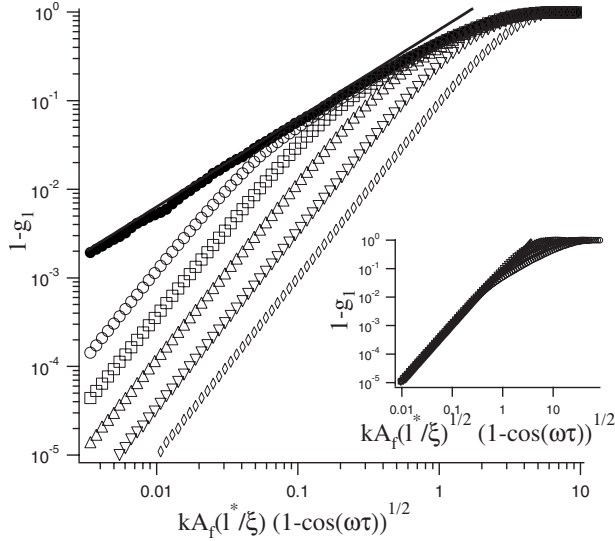


FIG. 7. Computed values of $1-g_1$ as a function $kA_f \frac{l^*}{\xi} \sqrt{1-\cos(\omega\tau)}$. Symbols are simulations at $\xi=l^*$ (\diamond), $\xi=3l^*$ (∇), $\xi=10l^*$ (\triangle), $\xi=30l^*$ (\square), $\xi=100l^*$ (\circ), and $\xi=\infty$ (\bullet) (affine deformation). Line is Eq. (15). Inset: same data except affine deformation, as a function of $kA_f \sqrt{l^*/\xi} \sqrt{1-\cos(\omega\tau)}$. Line is Eq. (14). Simulations shown are performed with $\omega\tau=\pi/2$, and simulations at $\omega\tau=\pi$ are identical.

function $g_1 = \langle e^{-\Delta\phi} \rangle$ is averaged over 100 values of t and 10^5 different paths.

We compute $1-g_1$ for different values of the amplitude kA_f and of ξ/l^* . Figure 7 shows results obtained for $\omega\tau=\pi/2$. We have performed simulations for $\xi/l^*=1, 3, 10, 30, 100$, and for an affine deformation corresponding to the limit $\xi/l^* \rightarrow \infty$. For the latter, we observe the behavior predicted by Eq. (15). For large values of ξ/l^* , the same behavior is also observed, but with a limited range of validity. At small values of ξ/l^* , $1-g_1$ varies quadratically with kA_f . Low-amplitude curves collapse on a master curve when plotted as a function of $kA_f \sqrt{l^*/\xi} / \sqrt{1-\cos(\omega\tau)}$, as expected by Eq. (14).

We have also studied photon random walks with correlated orientations of the different steps. Very little is known about the distribution of path lengths and scattering angles in foam. We consider a model of propagation with a constant deviation of angle θ between two successive steps. The path lengths are chosen according to one of the two following rules: In model (i) the length l of the steps is constant and taken as $l=l^*[1-\cos(\theta)]$. This gives a transport mean free path of $l/[1-\cos(\theta)]=l^*$. In model (ii), the length of every step is taken as $l=-l^* \ln(R) * [1-\cos(\theta)]$ with R a random number uniformly distributed between 0 and 1. The transport mean free path is also l^* .

Figure 8 shows the results of these simulations for correlated random walks with $\cos(\theta)=0.9$. This corresponds to random walks where 10 steps are necessary in order to loose the correlation of the orientation. For the two models shown here, the variations of g_1 expected from Eq. (14) are well followed. For an affine deformation, Eq. (15) is followed for these correlated random walks.

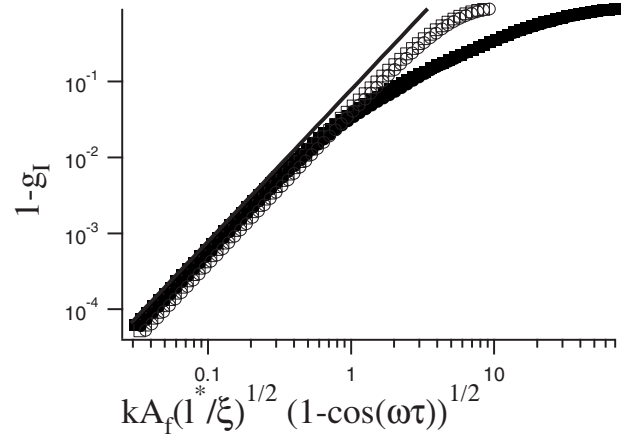


FIG. 8. Computed values of $1-g_1$ as a function of $kA_f \sqrt{l^*/\xi} \sqrt{1-\cos(\omega\tau)}$. Symbols are simulations: model (i) with $\cos(\theta)=0.9$, $\xi=l^*$ (\circ), $\xi=100l^*$ (\bullet), model (ii) with $\cos(\theta)=0.9$, $\xi=l^*$ (\square), $\xi=100l^*$ (\blacksquare). Line is Eq. (14). Simulations shown are performed with $\omega\tau=\pi/2$, and simulations at $\omega\tau=\pi$ are identical.

C. Remarks on the model

In this section, we have discussed the effect of a periodic shear on the coherence of the scattered electric field. We started this discussion by considering random walks with a succession of uncorrelated steps. In the case of an homogeneous deformation in the sample, we found [see Eq. (15)] that the decorrelation varies linearly with the shear rate which is proportional to A_f/ξ . This result has already been reported (see [26] when no Brownian motion of scatterers is present). The linearity of $1-g_1$ with A_f/ξ is also expected to hold even for correlated random walks of photons (see Appendix A of [26]). When the shear is localized in some part of the sample, photons “see” deformed and non deformed zones. In the case of random walks made of a succession of uncorrelated steps, analytical expansions may be obtained [see Eqs. (14) and (15)] which are in agreement with results of numerical simulations. When the random walk is made of steps whose orientations are strongly correlated, and made of steps of different lengths, numerical simulations show that Eqs. (14) and (15) are still satisfactory approximations for $1-g_1$. So, we may expect Eqs. (14) and (15) to give good approximations of $1-g_1$, even if details about the nature of the random walk in the foam are missing in the literature.

When the shear is concentrated near the surface where the light is backscattered, the variation of $1-g_1$ with A_f changes. One observes that the decorrelation is smaller than in the case of a homogeneous deformation (see Fig. 7). This arises because photons that penetrate deeply into the sample do not see an homogeneous deformation. These long paths dominate the decorrelation at small deformations.

IV. DISCUSSION

The theoretical approach presented above shows that depending on the distance ξ over which the foam is sheared, the electric field correlation functions are modulated with an amplitude that depends differently on the amplitude of the acoustic wave (i.e., linearly for large ξ or quadratically for

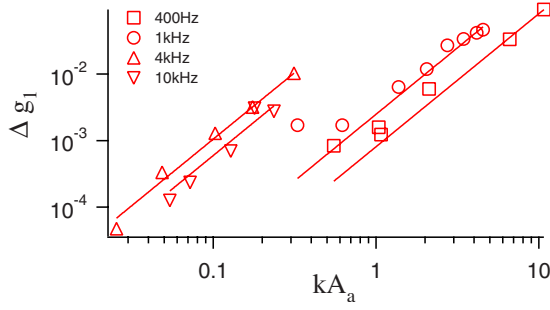


FIG. 9. (Color online) Plot of Δg_1 as a function of kA_a , where k is the optical wavevector and A_a is the acoustic displacement in air. Symbols are experimental data and lines are quadratic fits.

small ξ). In this section, we first investigate this dependence from the experimental data, showing that we are in the quadratic regime. In a second part, we propose a theoretical analysis describing the specific boundary conditions at the foam/wall interface for our experiment, and extract an expression for the localization length ξ . Finally, we compare this prediction to our experimental results.

A. Quadratic dependence of Δg_1 with the acoustic amplitude

We compute from the data the amplitude Δg_1 of the modulation of the electric field correlation function. The correlation functions of the scattered electric field and intensity are linked by the Siegert relation [24]:

$$g_2(\tau) = 1 + \beta |g_1(\tau)|^2, \quad (16)$$

where β is an experimental parameter fixed by the optical setup [24]. We first determine β as the limit $g_2(\tau \rightarrow 0) - 1$, and then we compute $g_1(\tau)$ from Eq. (16).

We define the amplitude Δg_1 of the modulation of $g_1(\tau)$ as follows:

$$\Delta g_1 = \frac{g_1^{\max,2} + g_1^{\max,3}}{2} - g_1^{\min}, \quad (17)$$

where $g_1^{\max,2}$ and $g_1^{\max,3}$ are the second and third maxima of g_1 , and g_1^{\min} is the minimum in-between (see Fig. 3). This definition corrects Δg_1 from a slow linear decrease in g_1 due to the foam aging.

Figure 9 is a log-log plot of Δg_1 as a function of kA_a for different values of the acoustic frequency. For each frequency, Δg_1 is found experimentally to vary quadratically with kA_a . As shown in Sec. III, this cannot be interpreted without supposing that the deformation of the foam must be localized in the vicinity of the wall, over a distance $\xi < \lambda_{acc}$.

Attention must be drawn on the following point: the controlled experimental parameter is the acoustic displacement A_a in air while the model developed in Sec. III considers the acoustic displacement A_f in the foam. Linking these two quantities requires a model for the transmission of sound from air to foam. We will treat this acoustic transmission as a linear phenomena so that the transmission coefficient from air to foam is independent of the sound amplitude. To our knowledge, no nonlinear transmission effect at an air/foam

interface has indeed been reported yet. We may first estimate the transmission coefficient at an air/foam interface $t_f = A_f/A_a$ for a plane wave under normal incidence. In this case, $t_f = 2/(1 + Z_f/Z_a)$, where $Z_f/Z_a = \sqrt{\rho_f \chi_a / \rho_a \chi_f}$ is the ratio of the acoustic impedances in the foam and in air, with ρ the density and χ the compressibility. We use Wood's model [33], which has been shown to describe relatively well the experimental measurements of ultrasound propagation through shaving foams [18]. This model relies on the mean-field approximation that the acoustic wavelength λ_{acc} is much larger than the bubble size D . This is verified in our case (see Sec. III), so that the use of Wood's model is justified. Accordingly, we use for the foam the simple averages: $\rho_f = \varepsilon \rho_w + (1 - \varepsilon) \rho_a \approx \varepsilon \rho_w$ and $\chi_f = \varepsilon \chi_w + (1 - \varepsilon) \chi_a \approx (1 - \varepsilon) \chi_a$, where the subscript w refers to water, and ε represents the liquid fraction. For the typical liquid fraction in our experiments, $\varepsilon \approx 10\%$, this gives $Z_f/Z_a \approx 10$ hence $t_f \approx 0.2$. This transmission coefficient does neither take into account diffraction at the entering in the foam cell, nor damping during the propagation in the foam. Thus, $t_f = 0.2$ is expected to be the maximum transmission coefficient.

We also need to check if we are in the required condition for Eq. (14) to be valid, i.e., $kA_f < 1$. For our experiment, the values of the acoustic displacement in the foam are then expected to be smaller than $t_f A_a$. In our case, the acoustic amplitude in air ranges from $0.02 < kA_a < 10$, and then $0.004 < t_f kA_a < 2$. Since we expect A_f to be less than or of the order of A_a , we may expect kA_f to be less than or of the order of unity. Thus, Eq. (14) should hold, and we expect:

$$\Delta g_1 = g_1(0) - g_1(\pi/\omega) = 0.156 (kA_f)^2 \frac{I^*}{\xi}. \quad (18)$$

This quadratic dependence of Δg_1 with the acoustic amplitude is the observed experimental behavior (see Fig. 9).

B. Shear length and no-slip boundary condition

The model of deformation used to compute theoretically and numerically the modulation of intensity correlation functions assumes that the foam shear is localized in a thin layer near the walls. This is also as evidenced by our experiments. The presence of such a sheared zone suggests that the foam is not free to move at the wall. This might appear surprising, since a glass boundary is usually considered as smooth, and hence slip is expected to occur on it. However, one shall be aware that the acoustic displacement is not quasistatic, so that viscous effects at the boundary must be taken into account. We now prove that due to the combination of high frequencies and tiny displacements specific to an acoustic forcing, the foam indeed displays an effective no-slip boundary condition, and we predict the length ξ over which the foam close to the wall is significantly sheared.

We quantify the motion of the foam by its displacement field. We assume that $\xi \ll \lambda_{acc}$; therefore, although the details of the acoustic field within the foam are unknown, at the length scale of ξ , it reduces to a uniform forcing $F \cos \omega t$ along one direction x : the displacement field is then of the form $x(z, t)$ (Fig. 10). We perform a force balance on a slice of foam of thickness dz , located at z , and parallel to the wall,

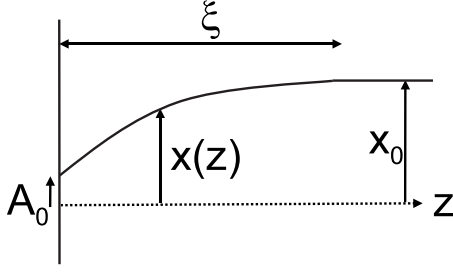


FIG. 10. Sketch of the displacement field in the foam, with the imposed acoustic displacement x_0 and the slip amplitude at the wall A_0 .

in the spirit of [34]. Because of the high acoustic frequency, we do not neglect inertia, contrary to what is often done for foams. The inertial contribution is balanced by a gradient of viscoelastic shear stress τ and by an acoustic forcing term. Hence, the force balance writes:

$$\rho_f \frac{\partial^2 x}{\partial t^2} = \frac{\partial \tau}{\partial z} + F \cos \omega t. \quad (19)$$

The order of magnitude of the foam displacement is given by the acoustic displacement $A_f = t_f A_a$, with $t_f \approx 0.2$ (see Sec. IV A) and the acoustic displacement in air, A_a , is given by Eq. (1). Taking the lowest frequency $f = 400$ Hz and the highest amplitude $A_{a,dB} = 90$ dB yields $A_f \approx 10^{-7}$ m. This is much shorter than all other relevant length scales, especially the bubble size and the acoustic wavelength, hence the strain $\gamma = \partial x / \partial z$ remains very small. Therefore, as usual in linear rheology, we assume a linear relationship between the shear stress and strain: $\tau = G\gamma = G \partial x / \partial z$, where $G = G' + iG''$ is the complex shear modulus. Writing $x(z, t) = \text{Re}[\underline{x}(z)e^{i\omega t}]$, Eq. (19) becomes:

$$\frac{\partial^2 \underline{x}}{\partial z^2} + \frac{\rho_f \omega^2}{G} \underline{x} = \frac{F}{G} = \frac{\rho_f \omega^2}{G} x_0. \quad (20)$$

At a distance from the wall much higher than ξ but much smaller than λ_{acc} , which is possible since $\xi \ll \lambda_{acc}$, shear vanishes and \underline{x} tends toward a constant x_0 , the local amplitude of acoustic displacement (Fig. 10). Then, Eq. (20) can be rewritten as:

$$\frac{\partial^2 \underline{X}}{\partial z^2} + \frac{\rho_f \omega^2}{G} \underline{X} = 0,$$

with $\underline{X} = \underline{x} - x_0$ and $\lim_{z/\xi \rightarrow \infty} \underline{X} = 0$. Hence, $\underline{X}(z) = X_0 e^{\kappa z}$, with κ the root with negative real part of the equation $\kappa^2 = -\rho_f \omega^2 / G$, i.e., $\kappa = -i\omega e^{-i\Delta/2} (\rho_f / |G|)^{1/2}$ with $\Delta = \arctan G'' / G'$. Hence, $\kappa = \kappa' + i\kappa''$ with $\kappa' = -\omega (\rho_f / |G|)^{1/2} \sin(\Delta/2)$ and $\kappa'' = -\omega (\rho_f / |G|)^{1/2} \cos(\Delta/2)$, thus $\underline{X}(z) = X_0 e^{-z/\xi} e^{i\kappa'' z}$ with the following prediction of the shear length:

$$\xi = -\frac{1}{\kappa'} = \frac{\sqrt{|G|}}{\omega \sqrt{\rho_f} \sin(\Delta/2)}. \quad (21)$$

This prediction relates the shear length and the shear modulus. To our knowledge, no direct measurement of the shear modulus has been performed for such high frequencies in foams. However, the following scaling has been proposed at high frequency [11]: $G = G_0(1 + (i\omega / \omega_c)^{1/2})$, and has been shown to apply well to Gillette foam with $G_0 = 2 \times 10^3$ dyn cm $^{-2} = 2 \times 10^2$ N m $^{-2}$ and $\omega_c = 2 \times 10^2$ rad s $^{-1}$ [4], at frequencies above 5 rad s $^{-1}$, up to a few 10^2 rad s $^{-1}$. In our experiments, $\omega \gg \omega_c$, hence we retain the simplified expression: $G \approx G_0 \sqrt{i\omega / \omega_c}$. Therefore, $|G| \approx G_0 \sqrt{\omega / \omega_c}$ and $\Delta \approx \pi/4$, thus:

$$\xi \approx \frac{\sqrt{G_0}}{\omega_c^{1/4} \omega^{3/4} \sqrt{\rho_f} \sin(\pi/8)}. \quad (22)$$

Computed values of ξ are 2.8, 1.4, 0.5, and 0.2 mm for $f = 0.4, 1, 4$ and 10 kHz, respectively: ξ is of the order of 1 mm, which means that the foam is sheared over typically ten layers of bubbles. The corresponding values of the acoustic wavelength $\lambda_{acc} = c/f$, with $c \approx 50$ m/s [18], are 12.5, 5, 1.25, and 0.5 cm: they are one to two orders of magnitude higher than ξ , which justifies our main approximation $\lambda_{acc} \gg \xi$.

To get a complete solution and quantify the amount of wall slip, we must apply the boundary condition at the wall. It results from a second force balance accounting for the inertia of the Plateau Borders (PBs) in contact with the wall (wall PBs), bubble/wall friction, and the bulk shear stress $\tau_{(z=0)}$, which acts as the driving force tending to drag the wall PBs:

$$\mu_{PB} \frac{\partial v}{\partial t} = \tau_{(z=0)} - \tau_W, \quad (23)$$

where μ_{PB} is the mass per unit surface of the wall PBs, $v = (\partial x / \partial t)_{z=0,t}$ the slip velocity, and τ_W the wall shear stress. Since the length of wall PBs per unit surface is of order $1/D$, and their mass per unit length is of order $\rho_w R_{PB}^2$ with $R_{PB} \approx D\sqrt{\varepsilon}$ the typical cross-section dimension of a wall PB, then $\mu_{PB} \approx \rho_f D$. For Gillette foam, the air/liquid interfaces are immobile [7], hence the wall shear stress is $\tau_W = \alpha \sigma \sqrt{Ca} / D$ [7] with α a numerical prefactor depending only on the liquid fraction; for $\varepsilon \approx 10\%$, we compute $\alpha \approx 2$ from Eq. (13) in [7]. The capillary number Ca is defined by: $Ca = \eta v / \sigma$, with $\eta \approx 10^{-3}$ Pa.s the liquid viscosity, and $\sigma \approx 30$ mN/m the surface tension. Hence, the force balance Eq. (23) yields:

$$\rho_f D \frac{\partial v}{\partial t} = G \gamma_{(z=0)} - \alpha \frac{\sqrt{\eta \sigma}}{D} \sqrt{v}.$$

Taking as an order of magnitude $v \approx \omega A_0$ with $A_0 = x_0 + X_0$ the amplitude of foam slip at the wall (Fig. 10), and $G \gamma_{z=0} = G(\partial x / \partial z)_{z=0} \approx |G| X_0 / \xi$, we get:

$$-\rho_f D \omega^2 A_0 = \frac{|G|(A_0 - x_0)}{\xi} - \alpha \frac{\sqrt{\eta\sigma}}{D} \sqrt{\omega A_0},$$

which becomes after some straightforward algebra:

$$(1 + \delta)A_0^2 - 2[(1 + \delta)x_0 + x_1]A_0 + x_0^2 = 0, \quad (24)$$

where the parameter $\delta = \rho_f D \omega^2 \xi / |G| = D / [\xi \sin^2(\pi/8)]$ [after Eq. (21)] compares the importance of the inertia of the wall PBs and of the bulk shear stress in the force balance Eq. (23). Since $D \approx 10^{-4}$ m and $\xi \approx 1$ mm, δ is of order unity. The length x_1 obeys: $x_1 = \alpha^2 \eta \sigma \omega \xi^2 / D^2 |G|^2 \approx \alpha^2 \eta \sigma \omega_c \xi^2 / D^2 G_0^2$. Taking $\xi \approx 1$ mm, we compute $x_1 \approx 6 \times 10^{-5}$ m. On the other hand, $x_0 \approx A_f \approx 10^{-7}$ m, hence $x_1 \gg (1 + \delta)x_0$. Under this simplifying assumption, the amplitude of slip, solution of Eq. (24), is:

$$A_0 \approx \frac{(1 + \delta)x_0^2}{2x_1} \ll x_0,$$

hence the amount of slip is negligible compared to the acoustic displacement. This finally proves that the foam displays an effective no-slip boundary condition.

This theoretical analysis deserves some comments. We have shown that there is shear localization at the wall, and no slip, despite the fact that the glass wall is smooth. 3D foam oscillatory shear experiments usually do not exhibit such shear localization. The localization mechanism in our experiments is actually rather specific, since the occurrence of no-slip and the importance of inertia are crucially related to the combination of high frequencies and small displacements which are classical in acoustics, but very unusual in classical shear rheometry, where much lower frequencies and higher displacements are applied. Anyway, this theoretical analysis supports the experimental data, where the quadratic modulation of g_2 implies occurrence of shear close to the wall.

C. Quantitative comparison between theory and experiments

The previous modeling has allowed us to extract theoretical values of the localization length ξ . We can now try to compare their orders of magnitude to our experimental data.

We measure from experimental data (Fig. 9) the ratio $S = \Delta g_1 / (kA_a)^2$. Applying Eq. (18), we obtain:

$$\frac{A_f}{A_a} \sqrt{\frac{l^*}{\xi}} \approx 2.5\sqrt{S} \quad (25)$$

Measured values of $2.5\sqrt{S}$ are 0.071 ($f=400$ Hz), 0.13 ($f=1$ kHz), 0.83 ($f=4$ kHz) and 0.61 ($f=10$ kHz). As shown in Sec. IV B, ξ is of the order of a few bubble diameters. With $\xi \lesssim 10D$, $l^* \approx 2.9D$, and $\frac{A_f}{A_a} = t_f = 0.2$, we obtain $\frac{A_f}{A_a} \sqrt{\frac{l^*}{\xi}} \lesssim 0.34$. This is in reasonable agreement with the measured values of $2.5\sqrt{S}$. Furthermore, these values are in qualitative agreement with the behavior expected from Eq. (22), i.e., that ξ decreases when the acoustic frequency increases. However, one must remain careful for further analysis given the crude approximations made to describe of the transmission of the acoustic wave. These could probably ex-

plain the observed discrepancies. It is indeed clear that, at low frequencies, the acoustic diffraction has to be taken into account in order to describe the penetration of the acoustic wave into the foam cell.

V. CONCLUSIONS AND OUTLOOK

We have shown that it is possible to monitor—by a multiple light scattering technique such as DWS—how an external acoustic signal induces bubble displacements inside a foam. Thanks to theoretical, numerical and experimental approaches, we have obtained original results and explanations of the observed features. We have determined the origins of the modulation seen in light scattering data, and in particular understood its amplitude and the nontrivial quadratic dependence with the acoustic amplitude. We have shown that such a dependence is the signature of a specific shear profile near the walls holding the foam. Theoretically, this specific profile can be explained by the importance of inertia in the high frequency regime in which our experiments are performed.

Quantitatively, the experimental results are also consistent with the theoretical estimations. In agreement with the predictions, we can extract from the data that the typical displacement in the foam is of the order of a few tens of nm, spread over a few bubble diameters, thus corresponding to deformation of the order of 10^{-4} .

Another interesting result is illustrated by the set of Eqs. (14) and (15): we have derived analytical results showing significant differences, in backscattering, between a sample undergoing an homogeneous constant shear and a sample in which sheared and nonsheared parts are present. On this specific question, performing DWS in backscattering and testing whether a modulation occurs linearly or quadratically with the amplitude of deformation (whatever its source) is then a possible way to investigate the spacial homogeneity of the deformation.

More generally, this study can be considered as a first landmark, already bringing some insights on some of the questions raised in the introduction: in particular, we have shown that an acoustic wave is actually an interesting way for applying controlled shear deformations on a foam, in this range of high frequencies and spatial extent which remains poorly understood. As well, on the foam acoustic issues, we have shown that DWS is a useful tool for extracting information at the scale of the bubble, probably crucial for explaining macroscopic sound attenuation and speed in foams.

At this stage, many possible developments can be proposed. One can first test other sample sizes and geometries for the input of light and sound. As well, it is interesting to test whether or not an acoustic perturbation could sufficiently deform the foam structure to eventually trigger some rearrangements of bubble (T1 event [3]). It should also be possible to perform the DWS measurements at different locations on a sample, and then to draw a map of the acoustic deformation.

Lastly, from a different point of view, our results also show that an acoustic signal can provide a significant (and possibly annoying) perturbation on a DWS correlation curve. Thus, to get clean measurements, one should minimize any extra acoustic or mechanical perturbations (at least for experiments with foams).

ACKNOWLEDGMENTS

This work has been supported by ANR under Grant No. “NewFoam”-Blan-07-340. We thank Valentin Leroy and Cyprien Gay for fruitful exchanges, and the GdR Mousses for providing a favorable framework for discussions.

-
- [1] S. Jurine, S. Cox, and F. Graner, *Colloids Surf., A* **263**, 18 (2005).
- [2] S. Hilgenfeldt, S. A. Koehler, and H. A. Stone, *Phys. Rev. Lett.* **86**, 4704 (2001).
- [3] D. J. Durian, D. A. Weitz, and D. J. Pine, *Phys. Rev. A* **44**, R7902 (1991).
- [4] A. D. Gopal and D. J. Durian, *Phys. Rev. Lett.* **91**, 188303 (2003).
- [5] H. A. Barnes, J. F. Hutton, and K. Walters, *An Introduction to Rheology* (Elsevier, Amsterdam, 1989).
- [6] R. Höhler and S. Cohen-Addad, *J. Phys.: Condens. Matter* **17**, R1041 (2005).
- [7] N. D. Denkov, S. Tcholakova, K. Golemanov, K. P. Ananthapadmanabhan, and A. Lips, *Soft Matter* **5**, 3389 (2009).
- [8] S. Marze, R. M. Guillemic, and A. Saint-Jalmes, *Soft Matter* **5**, 1937 (2009).
- [9] A. D. Gopal and D. J. Durian, *J. Colloid Interface Sci.* **213**, 169 (1999).
- [10] S. Marze, D. Langevin, and A. Saint-Jalmes, *J. Rheol.* **52**, 1091 (2008).
- [11] A. J. Liu, S. Ramaswamy, T. G. Mason, H. Gang, and D. A. Weitz, *Phys. Rev. Lett.* **76**, 3017 (1996).
- [12] P. Sollich, F. Lequeux, P. Hébraud, and M. E. Cates, *Phys. Rev. Lett.* **78**, 2020 (1997).
- [13] M. L. Falk and J. S. Langer, *Phys. Rev. E* **57**, 7192 (1998).
- [14] L. Bocquet, A. Colin, and A. Ajdari, *Phys. Rev. Lett.* **103**, 036001 (2009).
- [15] P. Saramito, *J. Non-Newtonian Fluid Mech.* **145**, 1 (2007).
- [16] W. Leutz and G. Maret, *Physica B* **204**, 14 (1995).
- [17] I. I. Goldfarb, I. R. Schreiber, and F. I. Vafina, *J. Acoust. Soc. Am.* **92**, 2756 (1992).
- [18] N. Mujica and S. Fauve, *Phys. Rev. E* **66**, 021404 (2002).
- [19] D. Bicoût, E. Akkermans, and R. Maynard, *J. Phys. I* **1**, 471 (1991).
- [20] D. Bicoût and R. Maynard, *Physica A* **199**, 387 (1993).
- [21] M. Erpelding, A. Amon, and J. Crassous, *Phys. Rev. E* **78**, 046104 (2008).
- [22] D. J. Pine, D. A. Weitz, J. X. Zhu, and E. Herbolzheimer, *J. Phys. (France)* **51**, 2101 (1990).
- [23] *Dynamic Light Scattering: The Method and Some Applications*, edited by W. Brown (Oxford University Press, New York, 1993).
- [24] B. J. Berne and R. Pecora, *Dynamic Light Scattering With Applications to Chemistry, Biology, and Physics* (Dover, New York, 2000).
- [25] X. Wu, D. Pine, P. Chaikin, J. Huang, and D. Weitz, *Opt. Soc. Am. B* **7**, 15 (1990).
- [26] D. Bicoût and G. Maret, *Physica A* **210**, 87 (1994).
- [27] L. Djaoui and J. Crassous, *Granular Matter* **7**, 185 (2005).
- [28] J. Crassous, *Eur. Phys. J. E* **23**, 145 (2007).
- [29] M. U. Vera, A. Saint-Jalmes, and D. J. Durian, *Appl. Opt.* **40**, 4210 (2001).
- [30] J. X. Zhu, D. J. Pine, and D. A. Weitz, *Phys. Rev. A* **44**, 3948 (1991).
- [31] *Conduction of Heat in Solids*, 2nd ed., H. S. Carslaw and J. C. Jaeger (Clarendon Press, Oxford, 1959).
- [32] A. S. Gittings, B. Bandyopadhyay, and D. J. Durian, *EPL* **65**, 414 (2004).
- [33] A. B. Wood, *A Textbook of Sound* (Bell and Sons, London, 1944), pp. 360–363.
- [34] G. Katgert, M. E. Möbius, and M. van Hecke, *Phys. Rev. Lett.* **101**, 058301 (2008).